Int. J. Microgravity Sci. Appl. 33(2) (2016) 330209
DOI: 10.15011/jasma.33.330209

IIIII ISPS-6 Proceedings IIIII
(Review)

Behavior of Fine Particle (Dust) Clouds in Plasmas under Gravity and Microgravity

Hiroo TOTSUJI[1], Kazuo TAKAHASHI[2] and Satoshi ADACHI[3]

Abstract

The behavior of fine particle (dust) clouds in plasmas is analyzed by theory, simulations, and experiments. The investigation is motivated by basic interest in strongly coupled Coulomb-like systems and by on-going experiments by PK-4 on-board the International Space Station (ISS). This apparatus succeeding PK-3 Plus has a different simple geometry and has a possibility to elucidate another fundamental aspects of fine particle systems in plasmas. We give an overview of the results of theoretical and simulation works and our experiments with the apparatus PK-4J which has a structure similar to PK-4.

Keyword(s): Fine particle (dusty) plasma, Fine particle (dust) cloud, PK-4, PK-4J
Received 29 September 2015; Accepted 15 February 2016; Published 30 April 2016

1. Introduction

Fine particles (dusts) of micrometer size in plasmas usually have charges of very large magnitude. Typical values are 10^3 to even 10^5 times the electronic charge. Because of strong interactions between charges and the possibility to observe positions and velocities of fine particles by the scattering of laser light, fine particle clouds have been attractive as objects of research for fundamental physics [1–3]. These particles, however, are still macroscopic and, in order to avoid the effect of gravity, experiments on the International Space Station (ISS) have been performed by the apparatus PKE-Nefedov and then PK-3 Plus [4].

After PK-3 Plus, the project PK-4 is now in progress [5]. In the apparatus PK-4, the plasma is generated by a discharge in a long cylindrical tube. This kind of plasma with the cylindrical symmetry and the uniformity along the axis may facilitate the observation of phenomena expected in three-dimensional homogeneous systems. We constructed PK-4J shown in Fig.1 whose structure is similar to PK-4.

Mainly supported by JAXA, we have been working on such cylindrical fine particle plasmas in order to propose possible interesting themes for PK-4 experiments as well as to make basic research on fine particle plasmas. We here overview the results of our theoretical, simulation, and experimental works [6–9].

We consider the stationary system of fine particles in a plasma with the cylindrical symmetry. The plasma is assumed to be generated by the discharge of the dc electric field along the axis. The average flow of the plasma is assumed to be suppressed by, for example, switching the polarity of the dc field. Typical values of parameters are plasma density of the order of $10^8 - 10^9 \mathrm{cm}^{-3}$, particle density $10^4 - 10^5 \mathrm{cm}^{-3}$, the electron temperature $1 - 3\mathrm{eV}$, and the ion and particle temperature 300 K.

We first describe the behavior of fine particle clouds in the continuum limit on the basis of the drift-diffusion equations [10]. We then give a framework to treat the effect of discreteness and describe the results of theory and simulations on structures. Some experimental results obtained on the ground and in the parabolic flights are also given.

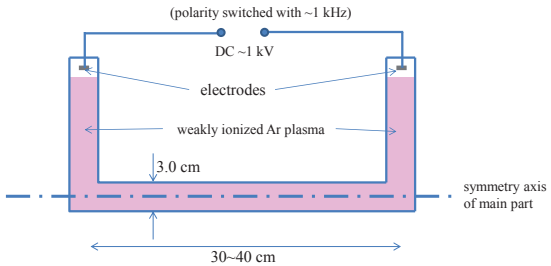

PK-4J

Fig. 1 In PK-4J, fine particles are observed in the central straight cylinder.

1 Okayama University
2 Kyoto Institute of Technology
3 JAXA/ISAS
(E-mail: totsuji-09@t.okadai.jp)

2. Basic Equations and General Properties of Solutions with Cylindrical Symmetry

2.1 Drift-Diffusion Equations

Our system is composed of plasma (electrons and ions) and fine particles. We denote physical quantities of each component by suffixes e, i, or α, α being the species of fine particles. They are in the atmosphere of neutral gas of typically 10-100 Pa. The inert gas is often adopted as the gas species and we assume Ar. Under typical conditions of experiments, ions, electrons, and fine particles experience frequent collisions with neutral gas atoms and are considered to be described by the diffusion coefficients $D_{e,i,\alpha}$ and the mobilities $\mu_{e,i,\alpha}$ which are related via the Einstein relations. As usually observed, each component has different temperatures, $T_{e,i,\alpha}$.

For densities $n_{e,i,\alpha}$ and flux densities $\mathbf{\Gamma}_{e,i,\alpha}$, we have equations of continuity,

$$\nabla \cdot \mathbf{\Gamma}_e = \nabla \cdot (-D_e \nabla n_e - \mu_e \mathbf{E}) = \frac{\delta n_e}{\delta t}, \tag{1}$$

$$\nabla \cdot \mathbf{\Gamma}_i = \nabla \cdot (-D_i \nabla n_i + \mu_i \mathbf{E}) = \frac{\delta n_i}{\delta t}, \tag{2}$$

and

$$\nabla \cdot \mathbf{\Gamma}_\alpha = \nabla \cdot (-D_\alpha \nabla n_\alpha + \mu_\alpha \frac{\mathbf{F}_\alpha}{Q_\alpha e}) = 0. \tag{3}$$

The right-hand sides express the generation and the loss of plasma. The force acting on a fine particle with the charge $-Q_\alpha e$, $\mathbf{F}_\alpha$, is given the electric field $\mathbf{E}$ and the ion drag force $\mathbf{F}_\alpha^{id}$;

$$\mathbf{F}_\alpha = (-Q_\alpha e)\mathbf{E} + \mathbf{F}_\alpha^{id}. \tag{4}$$

In our analysis, the average ion flow velocity u_i is smaller than the ion thermal velocity $v_i = (k_B T_i/m_i)^{1/2}$ and we adopt the expression for the ion drag force [2)]

$$F_\alpha^{id} \sim \frac{1}{3}\left(\frac{2}{\pi}\right)^{1/2} \frac{(Q_\alpha e)^2}{4\pi\varepsilon_0} \frac{n_i e^2}{\varepsilon_0 k_B T_i} \Lambda(\beta_T, r_\alpha/\lambda) \frac{u_i}{v_i}, \tag{5}$$

where $\Lambda(\beta_T, r_\alpha/\lambda)$ is the generalized Coulomb logarithm

$$-e^{\beta_T/2}\mathrm{Ei}(-\beta_T/2) + e^{[(\beta_T/2)(\lambda/r_\alpha)]}\mathrm{Ei}[-(\beta_T/2)(\lambda/r_\alpha)],$$

$\mathrm{Ei}(x)$ the exponential integral, and

$$\beta_T = \frac{|Q_\alpha| e^2/4\pi\varepsilon_0 k_B T_i}{\lambda} \tag{6}$$

(λ is the screening length in the plasma usually determined by the ion Debye wavenumber).

We introduce the factor f_α as the ratio of the magnitudes of the ion drag force to the electric field force defined by

$$f_\alpha = \frac{F_\alpha^{id}}{Q_\alpha e E}. \tag{7}$$

As for the generation/loss of plasma, we express the volume generation rate by $c_g n_e$ with the coefficient (constant) c_g. The plasma is lost by the recombination at the surface of fine particles and the boundary of the system (wall), the recombination in the bulk of plasma being neglected. The charge of the particle α is determined by the balance between the electron and the ion currents. Denoting the balanced current by c_α, we have the generation/loss of the plasma in the form

$$\frac{\delta n_i}{\delta t} = \frac{\delta n_e}{\delta t} = c_g n_e - \sum_\alpha c_\alpha n_\alpha. \tag{8}$$

The charge of a particle, which is approximately proportional to the radius and the electron temperature, is also influenced by the ion mean free path [2)]. We take the latter effect into account. In the following, we assume the cylindrical symmetry and denote the radius by R.

3. Behavior of Solutions

We here discuss the behavior of solutions analytically.

3.1 Without Dust Particles

In this case, the above equations reduce to well-known ones [11)] characterized by the distance $R_a = (D_a/c_g)^{1/2}$ determined by the rate c_g and the ambipolar diffusion coefficient D_a defined by

$$D_a = \frac{\mu_e D_i + \mu_i D_e}{\mu_e + \mu_i}. \tag{9}$$

The distribution is given by the Bessel function

$$n_e \sim n_i \sim n = n(R=0) J_0(R/R_a). \tag{10}$$

The normalized charge density around $R = 0$ is given by

$$0 < \frac{n_i(0) - n_e(0)}{n_e(0)} \sim \frac{T_e/T_i}{R_a^2 k_{Di}^2} \ll 1, \tag{11}$$

where $k_{Di} = [n_i(R=0)e^2/\varepsilon_0 k_B T_i]^{1/2}$ is the ion Debye wave number. The quasi-charge-neutrality holds, controlled by the factor $R_a^2 k_{Di}^2$ with a slightly positive net charge density around the axis.

3.2 Behavior near Axis

We now expand solutions with respect to R^2. When we have fine particles of one species α, we obtain well defined solutions with the the normalized charge density at $R = 0$ given by

$$\Delta = \frac{n_i(0) - n_e(0) - Q_\alpha(0) n_\alpha(0)}{n_e(0)} \sim \frac{d_1}{A}, \tag{12}$$

where

$$d_1 \sim \frac{T_e}{T_i}\left(1 - \frac{c_p}{c_g}\frac{n_p(0)}{n_e(0)}\right) \tag{13}$$

and

$$A \equiv R_a^2 \left[\frac{e^2 n_e(0)}{\varepsilon_0 k_B T_e} + \left(1 - f_p \frac{Q_p n_p}{n_i}\right)\frac{e^2 n_i(0)}{\varepsilon_0 k_B T_i}\right.$$

$$\left. + (1 - f_p)\frac{Q_p(0)^2 e^2 n_p(0)}{\varepsilon_0 k_B T_p}\right] \gg 1. \tag{14}$$

When $n_\alpha = 0$, A reduces to factor $R_a^2 k_{Di}^2$ and the solution reduces to the known result.

When

$$\frac{Q_p(0)^2 e^2 n_p(0)}{\varepsilon_0 k_B T_p} \gg \frac{e^2 n_i(0)}{\varepsilon_0 k_B T_i}\left(\gg \frac{e^2 n_e(0)}{\varepsilon_0 k_B T_e}\right), \tag{15}$$

we have $A \gg R_a^2 k_{Di}^2$ and therefore much enhanced charge neutrality. Densities are given by

$$\frac{n_e(s)}{n_e(0)} = 1 + a_1 \frac{R^2}{R_a^2} + \dots,$$

$$\frac{n_i(s)}{n_e(0)} = \frac{n_i(0)}{n_e(0)} + b_1 \frac{R^2}{R_a^2} + \dots,$$

$$\frac{n_p(s)}{n_e(0)} = \frac{n_p(0)}{n_e(0)} + c_1 \frac{R^2}{R_a^2} + \dots,$$

where

$$\frac{a_1}{b_1} \sim \frac{a_1}{Q_p(0)c_1} \sim \frac{n_e(0)}{Q_p^2(0) n_p(0)} \sim \frac{n_i(0)}{Q_p^2(0) n_p(0)} \ll 1$$

and

$$\frac{b_1}{Q_p(0)c_1} \sim 1.$$

We thus have (1) much enhanced charge neutrality, (2) almost flat electron distribution, and (3) the compensation of the change in fine particle charge by the change in ion density. Though the above analysis is for the case of cylindrical symmetry, we expect these features hold in the general case where we have appreciable amount of dust particles in the sense of (15). Though some of above characteristic have been observed in numerical simulations in the case of high particle density [12], the origin and the necessary condition have not been discussed.

3.3 Void Formation Condition

In experiments by PK-3 Plus, often observed is the central space called 'void' where we have no dust particles [13] due to the effect of the ion drag force [14]. Since we would like to have as large as possible systems of fine particles without void, the condition for the formation of voids is an important issue.

The void is considered to appear when the balance is lost between the inward force by the electric field and outward force by the ion drag for fine particles. The condition for the appearance of void may be given by

$$f_\alpha(0) = \left[\frac{F_\alpha^{id}}{Q_\alpha e E}\right]_{R\to 0} > 1 \quad \text{when} \quad n_\alpha(0) = 0. \tag{16}$$

This is rewritten in terms of basic parameters, for example,

$$n_e(0) > [n_e(0)]^c, \tag{17}$$

where $[n_e(0)]^c$ is expressed by r_α, T_e, and p_n (neutral gas pressure): The dependence of the particle charge number Q_α on these parameters needs to be taken into account.

3.4 Dust Particles of Two Species and Void-Like Structure

In the case where there exist dust particles of two species α and β with radii r_α and r_β, $r_\alpha > r_\beta$, both satisfying the no-void condition, we may have $1 > f^\alpha > f^\beta$ since the charge of a dust particle is proportional to its radius. The effect of ion drag on the species α is stronger than the one on the species β. The species α is then located in the outer domain and the species β is distributed in the inner domain. As a distribution of α, there is a void at the center filled with smaller fine particles of β.

4. Numerical Analyses of Drift-Diffusion Equations

Starting from the origin with some assumed value of Δ, we numerically integrate resultant equations and adjust Δ so as to have asymptotically vanishing distributions near the wall. Solutions are quite sensitive to the value of Δ and numerical computations with very high accuracy are needed. The radius of particles r_α is assumed to be $0.5 - 2$ μm.

Without fine particles, known solutions of ambipolar diffusion equation are reproduced. Though our equations are not expected to be applicable in the sheath domain near the wall, we obtain the solutions which can be smoothly connected to the domain.

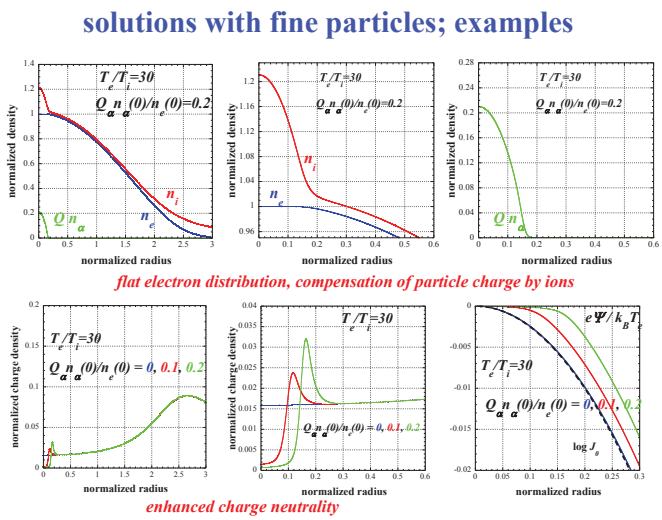

Fig. 2 Distribution of electrons, ions, and dust particles (top), charge density (bottom left and center), and electrostatic potential (bottom right)

4.1 Fine Particles of One Species

Some examples of distribution functions, the charge density, and the potential are shown in Fig.2. The radius of particle distribution increases with the density at the center. We observe that, when we have appreciable amount of fine particles, *the characteristics (1), (2), and (3) appear in the results of numerical integration.*

In addition, the net charge density overshoots to positive values at the radius where the density of dust particles vanishes and the electron distribution begins to decrease. Though the negative charge of dust particles is compensated by the increase of the ion density, the decay of dust particle density cannot be completely followed by the ions due to large difference in the diffusion coefficients, giving the positive peak in the net charge density.

4.2 Formation of Void

With the increase of the electron density (at the center) $n_e(0)$, the increase of the dust particle radius r_α, or the decrease of the neutral atom density (the gas pressure) p_n, there appears the void at the center. The critical values of the parameters are approximately expressed by

$$n_e^c(0)[\mathrm{cm}^{-3}] \sim 0.040 \cdot 10^8 \frac{p_n^{1.56}[\mathrm{Pa}]}{r_\alpha^{0.42}[\mu\mathrm{m}]T_e^{0.24}[\mathrm{eV}]}. \tag{18}$$

4.3 Dust Particles of Two Species

We have also analyzed some cases where there exist two species of dust particles. We observe that smaller particles are distributed inside of larger particles.

5. Framework to Describe Effects of Discreteness

The effective interaction between fine particles can be derived on the basis of the adiabatic approximation which regards the ambient plasma as a medium. After statistically averaging with respect to electrons and ions, the effective interaction between fine particles is given by the Helmholtz free energy for given configuration of fine particles [9].

We take advantage of the fact that, in our system, the size of the system L, the mean distance between particles a_p, and the mean distances between electrons or ions $a_{e,i}$ and satisfy the inequality $L \gg a_p \gg a_{e,i}$. We define the local average of a quantity $A(\mathbf{r})$ at $\mathbf{r}$, $\overline{A}(\mathbf{r})$, by

$$\overline{A}(\mathbf{r}) \equiv \frac{1}{\ell^3} \int_{\ell^3 \text{ centered at } \mathbf{r}} A(\mathbf{r}) d\mathbf{r}, \tag{19}$$

where ℓ satisfies $L \gg \ell \gg a_p \gg a_{e,i}$. The fluctuation $\delta A(\mathbf{r})$ is defined by

$$\delta A(\mathbf{r}) \equiv A(\mathbf{r}) - \overline{A}(\mathbf{r}). \tag{20}$$

The quantities in the continuum limit appeared in the previous sections correspond to the averages (which need bars in the notation of this section).

The total charge density $\rho(\mathbf{r})$ is written as

$$\rho(\mathbf{r}) = \rho_p(\mathbf{r}) + \rho_{bg}(\mathbf{r}) + \rho_{ext}(\mathbf{r}),$$

where $\rho_p(\mathbf{r})$ is the charge density of particles,

$$\rho_p(\mathbf{r}) = (-Qe) n_p(\mathbf{r}) = (-Qe) \sum_{i=1}^{N} \delta(\mathbf{r} - \mathbf{r}_i),$$

$\rho_{bg}(\mathbf{r})$ is the charge density of the background plasma composed of electrons and ions,

$$\rho_{bg}(\mathbf{r}) = (-e) n_e(\mathbf{r}) + e n_i(\mathbf{r}),$$

and $\rho_{ext}(\mathbf{r})$ is the external charge density or the source of the external field. From the Poisson's equation for the electrostatic potential $\Psi(\mathbf{r})$, we have

$$-\varepsilon_0 \Delta \overline{\Psi}(\mathbf{r}) = \overline{\rho}(\mathbf{r}) = \overline{\rho_p}(\mathbf{r}) + \overline{\rho_{bg}}(\mathbf{r}) + \rho_{ext}(\mathbf{r}),$$

and

$$-\varepsilon_0 \Delta \delta\Psi(\mathbf{r}) = \delta\rho_p(\mathbf{r}) + \delta\rho_{bg}(\mathbf{r}),$$

where $\delta\rho_{bg}(\mathbf{r}) = e[-\delta n_e(\mathbf{r}) + \delta n_i(\mathbf{r})]$.

As for the polarization of electrons and ions, we adopt the approximation of the linear adiabatic response to the local potential fluctuation $\delta\Psi(\mathbf{r})$:

$$\delta n_e(\mathbf{r}) \sim \overline{n_e}(\mathbf{r}) \frac{e\delta\Psi(\mathbf{r})}{k_B T_e}, \quad \delta n_i(\mathbf{r}) \sim -\overline{n_i}(\mathbf{r}) \frac{e\delta\Psi(\mathbf{r})}{k_B T_i}.$$

We then have

$$\delta\rho_{bg}(\mathbf{r}) = -\varepsilon_0 k_D^2(\mathbf{r})\delta\Psi(\mathbf{r}),$$

and the Poisson's equation for $\Delta\Psi$ reduces to

$$-\varepsilon_0[\Delta - k_D^2(\mathbf{r})]\delta\Psi(\mathbf{r}) = \delta\rho_p(\mathbf{r}).$$

Here, $k_D(\mathbf{r})$ is the (local) Debye wave number defined by

$$k_D^2(\mathbf{r}) = \frac{e^2\overline{n_e}(\mathbf{r})}{\varepsilon_0 k_B T_e} + \frac{e^2\overline{n_i}(\mathbf{r})}{\varepsilon_0 k_B T_i}.$$

For typical electron and ion temperatures, we can thus regard that the length ℓ satisfies the inequality $L \gg \ell \gg \{1/k_D,\ a_p\} \gg a_{e,i}$. Since the position dependence of $1/k_D$ is characterized by L and $L \gg 1/k_D$, we can write the approximate solution for $\delta\Psi(\mathbf{r})$ in the form

$$\delta\Psi(\mathbf{r}) \sim \int d\mathbf{r}' u(\mathbf{r},\mathbf{r}')\delta\rho_p(\mathbf{r}'),$$

where

$$u(\mathbf{r},\mathbf{r}') = \frac{\exp(-k_D^+|\mathbf{r}-\mathbf{r}'|)}{4\pi\varepsilon_0|\mathbf{r}-\mathbf{r}'|}$$

and $k_D^+ = k_D[(\mathbf{r}+\mathbf{r}')/2]$.

After some manipulations, the Helmholtz free energy is finally given by

$$U_{ex} = F_{id,0} + \frac{1}{2}\int d\mathbf{r}[\overline{\rho_p}(\mathbf{r}) + \overline{\rho_{bg}}(\mathbf{r}) + \rho_{ext}(\mathbf{r})]\overline{\Psi}(\mathbf{r})$$

$$+\left[\frac{1}{2}\sum_{i\neq j}^{N}(Qe)^2 u(\mathbf{r}_i,\mathbf{r}_j) + \sum_{i=1}^{N}(-Qe)\int d\mathbf{r}' u(\mathbf{r}_i,\mathbf{r}')[-\overline{\rho_p}(\mathbf{r}')]\right]$$

$$+\frac{1}{2}\int\int d\mathbf{r}d\mathbf{r}' u(\mathbf{r},\mathbf{r}')\overline{\rho_p}(\mathbf{r})\overline{\rho_p}(\mathbf{r}') - \frac{1}{2}\sum_{i=1}^{N}\frac{(Qe)^2 k_D(\mathbf{r}_i)}{4\pi\varepsilon_0}. \tag{21}$$

The averages $\overline{\rho_p}(\mathbf{r}), \overline{\rho_{bg}}(\mathbf{r})$, and $\overline{\Psi}(\mathbf{r})$ are determined so as to be consistent with the plasma generation and loss and the ambipolar diffusion in the system (and also with the external potential, if any). Configuration-dependent terms in (21),

$$\frac{1}{2}\sum_{i\neq j}^{N}(Qe)^2 u(\mathbf{r}_i,\mathbf{r}_j) + \sum_{i=1}^{N}(-Qe)\int d\mathbf{r}'[-\overline{\rho_p}(\mathbf{r}')]u(\mathbf{r}_i,\mathbf{r}')$$

$$-\frac{1}{2}\sum_{i=1}^{N}\frac{(Qe)^2 k_D(\mathbf{r}_i)}{4\pi\varepsilon_0}, \tag{22}$$

describe the interaction and potential for fine of particles at $\{\mathbf{r}_i\}_{i=1,\ldots N}$. The integral in the second term,

$$\int d\mathbf{r}'\frac{[-\overline{\rho_p}(\mathbf{r}')]}{4\pi\varepsilon_0|\mathbf{r}_i-\mathbf{r}'|}\exp(-k_D^+|\mathbf{r}_i-\mathbf{r}'|), \tag{23}$$

can be regarded as the Yukawa potential at $\mathbf{r}_i$ due to $[-\overline{\rho_p}(\mathbf{r}')]$, the (imaginary) charge density, which exactly cancels the average particle charge density $\overline{\rho_p}(\mathbf{r}')$, the *"shadow"* of $[\overline{\rho_p}(\mathbf{r}')]$. It is to be noted that the potential due to the shadow is *attractive* for particles. *Particles are thus mutually interacting via the Yukawa repulsion and, at the same time, confined by the attractive potential due to the shadow charge density* $[-\overline{\rho_p}(\mathbf{r}')]$. The last term in (22) is the free energy stored in the sheath around each particle (a one-body potential) giving the 'polarization force'.

Let us assume $\rho_{ext} = 0$. Even in this case, it is not easy to obtain the consistent distribution of plasma and particles.

When $(Qn_p)/n_e$ becomes nonnegligible compared with $1/(k_{De}R_a)^2$, we have to couple the particle charge density with the potential and therefore with electron and ion distributions. As shown in previous sections, the electrostatic potential becomes flatter in the domain where we have appreciable amount of particle charge: The charge neutrality is controlled by the factor A which includes the contribution from particles and can be much larger the case without particles. Then the simplest approximation in this case may be to assume that the potential is completely flat where particles exist [**Approximation 1**]. In our previous analyses of structures and ordering of particles in finite systems,[15,16] we have assumed that the average particle distribution is uniform with finite extensions. Noting the behavior of the potential with the existence of particles, we may expect this treatment to be close to reality when we have *appreciable* amount of particles.

On the other hand, when the contribution of particles to the net charge density is negligible, the plasma distribution and electrostatic potential are determined independently of particles. The potential is approximately expressed by [11]

$$\overline{\Psi}(R) \sim \frac{k_B T_e}{e}\ln J_0(R/R_a) = -\frac{k_B T_e}{e}\left(\frac{R^2}{4R_a^2} + \cdots\right). \tag{24}$$

In this case [**Approximation 2**], particles are considered to be in this parabolic electrostatic potential as in the model adopted in previous approaches[17–19]. This assumption has the advantage that the radius of the system is determined only by the number of particles.

6. Particle Simulation

On the basis of the theoretical framework given above, we analyze structures of fine particle clouds in cylindrical discharge like PK-4 and PK-4J.

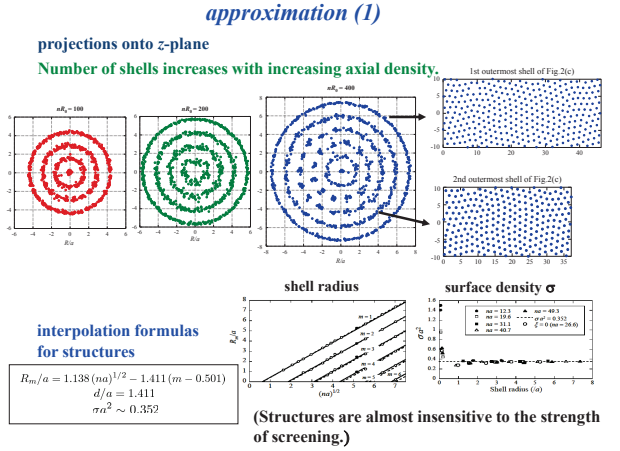

Fig. 3 Examples of shell structures in uniform cylinder (projection onto the cross section)

6.1 Flat Potential

Since it has been shown that the very existence of fine particles leads to almost flat electrostatic potential, one of reasonable assumptions is **Approximation 1**. At sufficiently low temperatures, fine particles are organized into shell structures [15]. Examples are shown in Fig.3. It has been shown that these structures are expressed by simple interpolation formulas to a good accuracy.

When the density of fine particles is negligibly small, we have the ambipolar field (24) and **Approximation 2** applies. With increased fine particle density, the distributions of plasma and fine particles have to be determined self-consistently. The average charge density becomes the source of the external electrostatic potential and the 'shadow' also contribute to confine particles. Since it is rather difficult to accurately estimate the electrostatic potential or the contribution from the 'shadow' self-consistently, we may evaluate two extreme cases, **Approximation 1** and **Approximation 2**.

However, we have some results (though not quantified enough) which indicate that the structure relative to the system radius is not so sensitive to the exact form of the potential. In addition, we do not have simple method to determine the extension of the system self-consistently. We therefore adopt **Approximation 2** in our simulations on the effects of gravity and the anisotropy of interaction.

6.2 Distribution in Ambipolar Potential and Effect of Gravity

In Fig.4, we show some structures of dust particles in the ambipolar potential. Note that the almost equal spacing between shells is also realized in this potential. With the increase of the gravity perpendicular to the symmetry axis, the structure moves downward as a whole and the shells become compressed in the direction of the gravity as naturally expected.

When we have mixtures of dust particles of different radii, they are separated by gravitation, even if the difference is rather small as also shown in Fig.4. In experiments, the system sometimes becomes a mixture of dust particles which are introduced and those non-intentionally exist.

6.3 Effect of Anisotropic Interaction

In our system, we have the flow of plasma along the axis with alternating direction. It is known that, due to such a flow of ions, the interaction between dust particles has an anisotropic part approximately expressed by [3]

$$-cM_t^2 \frac{(Q_\alpha e)^2}{r_{ij}^3} \exp(-r_{ij}/\lambda)(3\cos^2\theta_{ij} - 1), \tag{25}$$

where θ_{ij} is the angle between $\mathbf{r}_{ij}$ and the axis. The typical value of the ion thermal Mach number M_t is estimated to be around 0.5 from the discharge current of the order of 1 mA.

Structures of dust particles reflect the anisotropic part in their mutual interaction. An example is shown in Fig.5 where shells are developed into planes for observation of configuration on shells. We observe that the triangular lattice with defects in the case of Yukawa interaction becomes oriented along the axis. When looked at along the direction of the axis, shells are decomposed into points, or uniformly distributed points on the circle are changed into lumps of dots on almost the same circle. The projected shell structure seems to change from concentric shells into a kind of lattice of lumps.

7. Experiments

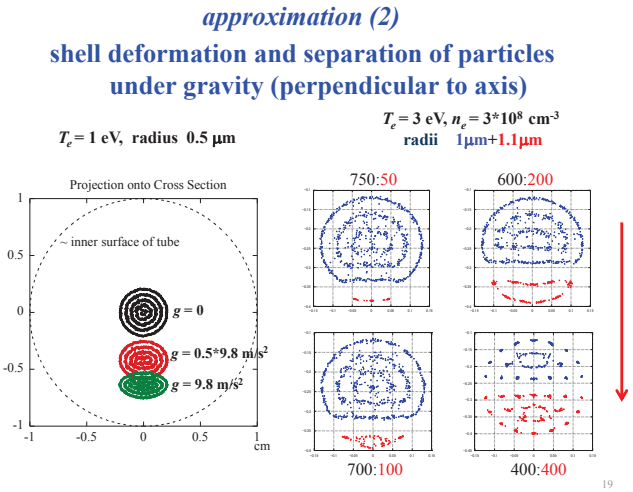

Fig. 4 Deformation and shift of center (left) and separation of particles with different radii

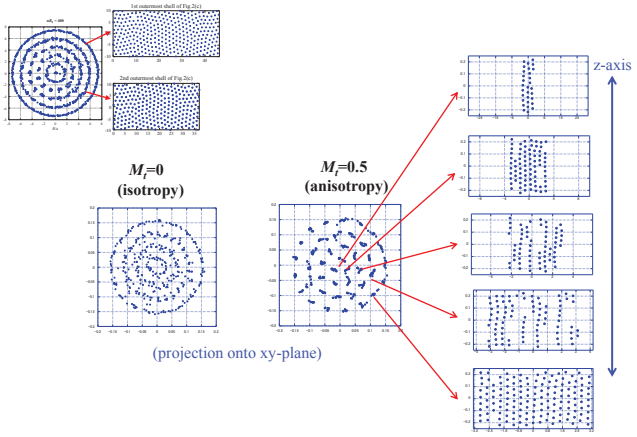

Fig. 5 Example of effect of anisotropic interaction. Cross sectional projection without anisotropic interaction (left), the one with anisotropic interaction (center), and cylinders (shells) cut-out into planes (right)

We performed experiments by PK-4J both on the ground and in the parabolic flights. We adopt Ar as the gas species and fine particles of the radius 1.3 μm are injected into the cylindrical plasma produced by the DC discharge along the axial direction with the polarity switched by 1 kHz. The switching is intended to suppress the overall motion of the plasma along the axis.

We have performed several sets of experiments. In experiments of 2011 and 2012, the images of particles are not sufficiently resolved. Examples are shown in Fig.6. In the parabolic flight, we have circular cross sections and under the effect of gravity which is perpendicular to the axis, we observe overall downward displacement and deformed shells compressed in the direction of the gravity. Though not sufficiently resolved, the structure is qualitatively consistent with the results of numerical simulations.

Experiments on the ground, deformed shell structure has been observed [20]. In our experiments [8], distributions of particles with circular cross section are observed under microgravity and deformed shells are observed on the ground. Our results seem to be not inconsistent with our theoretical works. For exact comparisons, however, some further improvement might be necessary.

In experiments of 2013 shown in Fig.7, the positions of fine particles are obtained. In this case, the distribution in the cross section is somewhat different from the ones obtained by simulations without anisotropic interaction and particles are observed to be aligned along the axis. Though further investigation is necessary, this might indicate the effect of anisotropic component in the mutual interaction. The distribution of probably heavier component under the gravity which are included not intentionally seems to be not simply accounted for.

8. Concluding Remark

We have briefly summarized our researches on fine particle plasmas with cylindrical symmetry which are still in progress. We hope them to be of some help to understand fundamental physics of strongly coupled charged particle systems.

Acknowledgments

The authors would like to thank members of ESA PK-4 Project at DLR and JIHT for useful information. They also thank the ISS Science Project Office of JAXA for kind support throughout this work and JAXA Working Group members for discussions.

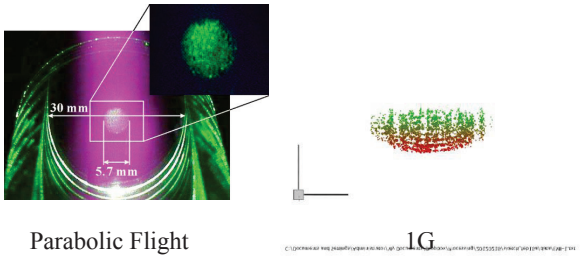

Fig. 6 Fine particles in PK-4J in parabolic flight (left) and under the downward gravity (right).

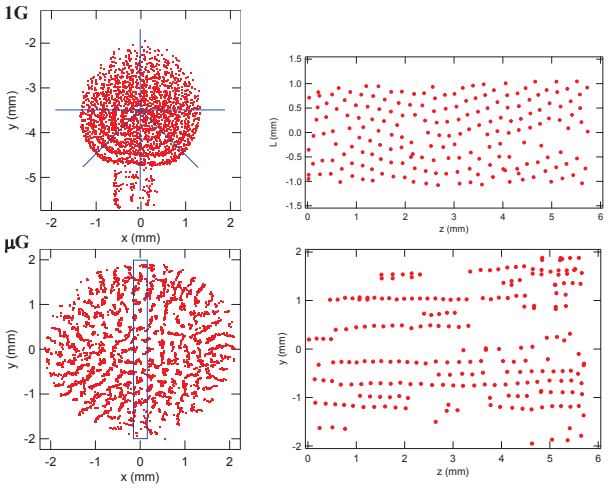

Fig. 7 Fine particles under the downward gravity (upper) and in parabolic flight (lower). Projection onto the cross section (left), development of outermost shell (upper right), and distribution in the slice (lower right).

References

1) P. K. Shukla and A. A. Mamun, *Introduction to Dusty Plasma Physics* (Institute of physics Publishing, London, 2002).
2) V. E. Fortov, A. V. Ivlev, S. A. Khrapak, A. G. Khrapak, and G. E. Morfill, Physics Reports, **421**, 1(2005).
3) G. E. Morfill and A. V. Ivlev, Rev. Mod. Phys. **81**, 1353(2009).
4) H. M. Thomas, G. E. Morfill, V. E. Fortov, A. V. Ivlev, V. I. Molotkov, A. M. Lipaev, T. Hagl, H. Rothermel, S. A. Khrapak, R. K. Suetterlin, M. Rubin-Zuzic, O. F. Petrov, V. I. Tokarev, and S. K. Krikalev, New J. Phys. **10**, 033036(2008).
5) V. Fortov, G. Morfill, O. Petrov, M. Thoma, A. Usachev, H. Höfner, A. Zobin, M. Kretschmer, S. Ratynskaia, M. Fink, K. Tarantik, Yu. Gerasimov, and V. Esenkov, Plasma Phys. Control. Fusion **47**, B537(2005).
6) H. Totsuji, J. Plasma Phys. **80**, 843(2014); H. Totsuji, Plasma Phys. Control. Fusion **58**, 045010(2016).
7) H. Totsuji, C. Totsuji, K. Takahashi, and S. Adachi, Int. J. Microgravity Sci. Appl. **31**, 55(2014).
8) K. Takahashi, M. Tonouchi, S. Adachi, and H. Totsuji, Int. J. Microgravity Sci. Appl. **31**, 62(2014).
9) H. Totsuji, J. Phys. Soc. Jpn. **84**, 064501(2015).
10) For example, V. Land and W. J. Goedheer, New J. Phys. **8** 8(2006).
11) For example, F. Llewellyn-Jones, *The Glow Discharge and Introduction to Plasma Physics*, (Methuen, London, 1966), Chapter 6; F. F. Chen, *Introduction to Plasma Physics*, (Plenum Press, New York, 1974), Chapter 5.
12) D. N. Polyakov, V. V. Shumova, L. M. Vasilyak, and V. E. Fortov, Physica Scripta **82**, 055501(2010); D. N. Polyakov, V. V. Shumova, L. M. Vasilyak, and V. E. Fortov, Physics Letters A **375**, 3300(2011); G. I. Sukhinin, A. V. Fedoseev, S. N. Antipov, O. F. Petrov, and V. E. Fortov, Phys. Rev. E **87**, 013101(2013).
13) G. E. Morfill, H. M. Thomas, U. Konopka, H. Rothermel, M. Zuzic, A. Ivlev, and J. Goree Phys. Rev. Lett. **83**, 1598(1999).
14) J. Goree, G. E. Morfill, V. N. Tsytovich, S. V. Vladimirov, Phys. Rev. E **59**, 7055(1999).
15) H. Totsuji and C. Totsuji, Phys. Rev. E **84**, 045401(R)(2011).
16) H. Totsuji, C. Totsuji, T. Ogawa, and K. Tsuruta Phys. Rev. E **71**, 045401(R)(2005); H. Totsuji, T. Ogawa, C. Totsuji, and K. Tsuruta Phys. Rev. E **72**, 036406(2005).
17) C. Henning, H. Baumgartner, A. Piel, P. Ludwig, V. Golubnichiy, M. Bonitz, and D. Block, Phys. Rev. E **74**, 056403 (2006).
18) H. Kählert, P. Ludwig, H. Baumgartner, M. Bonitz, D. Block, S. Käding, A. Melzer, and A. Piel, Phys. Rev. E **78**, 036408 (2008).
19) F. Gu, H.-J. Wang, and J.-T. Li, Phys. Rev. E **85**, 056402 (2012).
20) S. Mitic, B. A. Klumov, U. Konopka, M. H. Thoma, G. E. Morfill Phys. Rev. Lett. **101**, 125002(2008).